Electrochimica Acta 56 (2011) 9426–9432

Contents lists available at ScienceDirect

Electrochimica Acta

journal homepage: www.elsevier.com/locate/electacta

Electrochemical synthesis of novel π-extended phenoxazine derivatives of porphyrincatecholes

Samira Osati, Saied Saeed Hosseiny Davarani*, Nasser Safari*, Mohammad Hossein Banitaba

Department of Chemistry, Faculty of Science, Shahid Beheshti University, G.C, Evin, 1983963113 Tehran, Iran

ARTICLE INFO

Article history:
Received 19 March 2011
Received in revised form 9 August 2011
Accepted 9 August 2011
Available online 19 August 2011

Keywords:
Porphyrins
Catechol
Phenoxazine
Electrosynthesis
Nanostructure

ABSTRACT

Three new functionalized phenoxazine-catechol porphyrins **7a–c** have been synthesized by a green one-pot method and structurally characterized by spectroscopic analysis. The electro-oxidation of 5,10,15,20-tetrakis(2,3-dihydroxyphenyl) porphyrins(**1a–c**) with four catechol units in the presence of 2-aminophenol **8** as bidentate nucleophile has been done and phenoxazine rings have been formed by intermolecular and intramolecular Michael addition reactions. Spectroscopic characterization and voltammetry results have allowed us to propose four independent *ECEC* mechanisms for the electrochemical oxidation pathway. The functionalization of the porphyrins affected their photophysical properties. Expansion of the UV–vis spectrum range and the decrease of the fluorescence intensity of the products would support the energy transfer between the porphyrin core excited states to the four substitutions as the electron acceptor subunits. SEM images indicate that this method produces regularly shaped manganese porphyrin nano-particles **7c** that possess a cubic nano structure.

© 2011 Elsevier Ltd. All rights reserved.

1. Introduction

Porphyrins are macrocyclic compounds with highly π-conjugated systems exhibiting intense absorption in the visible region. They are also widely found in nature. They catalyze enzymatic reactions and transport oxygen in the human body [1] and play an important role in photosynthesis. There has been continuous interest in the synthesis of porphyrins because of their potential applications in catalysis, medicine, photochemical energy conversion, molecular switches, and molecular electronics [2–5].

More than 70 different metal ions can form complexes with porphyrin rings and their physical and chemical properties can be easily tuned by peripheral substituent modifications or metal complexations. As a result, the diversity of synthetic routes towards functionalized porphyrins has expanded rapidly [6–11].

Functionalization of porphyrins has been obtained via different methods. We have endeavored to develop a synthetic strategy that enables the use of readily prepared porphyrins that are capable of being simply converted to a wide variety of functional groups. The key to such a system is the use of a porphyrin with oxidizable substituents as the starting material in the presence of diverse nucleophiles, to provide a variety of functionalized porphyrins.

Electrosynthesis is perhaps the most selective, green and simple method. Tetra phenyl porphyrins with two adjacent hydroxyl groups on each phenyl rings, actually have four units of catecholes. Catecholes units in these compounds can be electrochemically oxidized to very reactive forms of o-quinones with a total of eight electrophilic reactive sites that would be attacked by various nucleophiles [12–18]. Using 2-aminophenol **8** as a bidentate nucleophile leads to the formation of six member hetrocycles of phenoxazine derivatives of porphyrins. Phenoxazine derivatives have been widely investigated and have been shown to be an effective material as antitumor, antileukemia, and antimicrobial drugs [19,20]. They have also been used as biological stains, laser dyes, indicators and especially as chromospheres in antenna systems [21–25]. Since hydroxyl-phenyl substituted porphyrins were developed as potential new photo sensitizers for photodynamic therapy, the joining of four phenoxazine rings to the meso position of the porphyrins can increase their applicability in cancer therapy [26].

We used water and ethanol as safe and environment-benign solvents and designed an energy efficient process by performing the reaction at ambient temperatures and pressures; therefore this is a green synthetic method for porphyrin functionalization.

The present work develops a facile method for functionalizing porphyrins and the synthesis of new phenoxazine-porphyrin catechol derivatives (shown in Scheme 1) with good yields and purity. These compounds display unique properties accounting for their potential applications in chemistry, medicine, and physics.

2. Experimental

2.1. Apparatus and reagents

Cyclic voltammetry and controlled potential coulometry were performed using a μ-Autolab potentiostat/galvanostat. The

* Corresponding authors. Tel.: +98 2129902890; fax: +98 21 22403041.
E-mail address: n-safari@cc.sbu.ac.ir (N. Safari).

0013-4686/$ – see front matter © 2011 Elsevier Ltd. All rights reserved.
doi:10.1016/j.electacta.2011.08.030

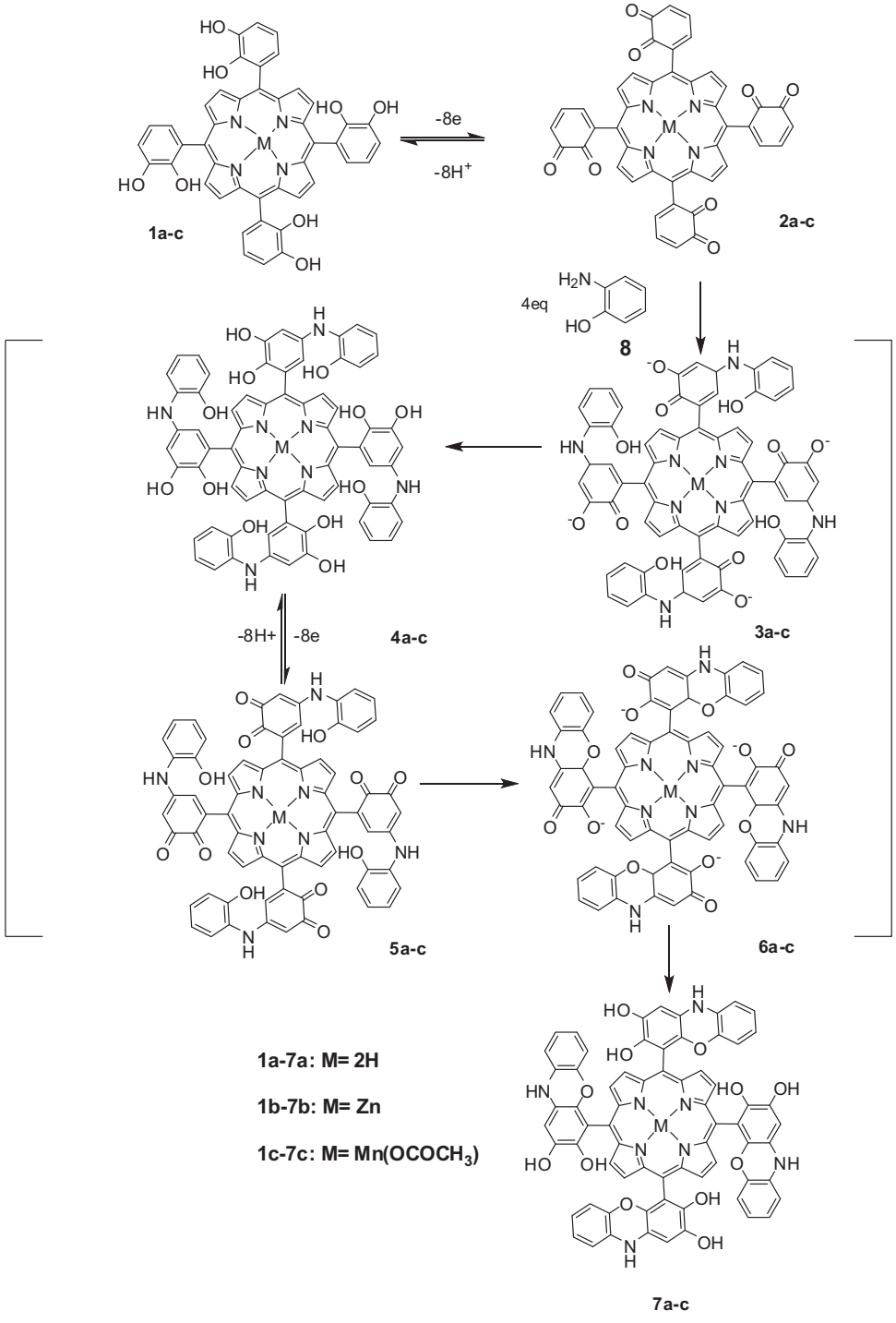

Scheme 1. Synthetic route for preparing of **7a–c** (proposed intermediates have been placed in brackets).

preparative electrolysis experiments were carried out with a Zahner potentiostat/galvanostat. The working electrode used in the voltammetry experiments was a glassy carbon disc (1.8 mm diameter) and a platinum wire was used as the counter electrode. The working electrode used in the controlled potential coulometry and milli mole scale electrolysis was an assembly of four graphite rods (10 mm diameter and 6 cm length) and a large surface platinum gauze constituted the counter electrode (graphite rods from Azar electrode, Uromieh, Iran and all other electrodes from Metrohm). The working electrode potentials *E* were measured versus 3 M Ag/AgCl as reference electrode. ^{1}H NMR and ^{13}C NMR spectra were recorded using a 300 MHz Bruker instrument. Mass spectra were obtained by a matrix assisted laser desorption ionization-time of flight mass spectroscopy (MALDI-TOF-MAS) on a Kratos Kompakt MALDI-TOF-MS in reflectron mode. UV–vis spectra were recorded on a Shimadzu 2100 spectrophotometer using a 1 cm path-length cell. Infrared spectra were obtained on a Bomem FT-IR 470 spectrophotometer. Fluorescence spectra were recorded on a Perkin Elmer LS45 Fluorescence spectrometer.

All solvents and chemicals (pyrrole, BF_3etherate, 2,3-dimethoxybenzaldehyde, 3,4,5,6-tetrachloro-1,2-benzoquinone (*p*-chloranil), manganese (III) acetate, zinc(II)acetate, boron

tribromide and 2-aminophenol **8**) were reagent grade and purchased from Merck. A solution of phosphate buffer in water/ethanol (50/50, v/v) (0.1 M, pH = 7.5) was prepared.

5,10,15,20-Tetrakis (2,3-dihydroxyphenyl) porphyrin **1a**, 5,10,15,20-tetrakis(2,3-dihydroxyphenyl) porphyrin zinc (II) chloride **1b** and 5,10,15,20-tetrakis(2,3-dihydroxyphenyl) porphyrin manganese (III) acetate **1c** were prepared by demethylation reaction between their methoxy form (5,10,15,20-tetrakis(2,3-dimethoxyphenyl) porphyrin, 5,10,15,20-tetrakis(2,3-dimethoxyphenyl) porphyrin zinc (II)) chloride and 5,10,15,20-tetrakis(2,3-dimethoxyphenyl) porphyrin manganese (III) acetate and BBr_3 according to literature [27,28].

2.2. Electrosynthesis of *7a–c*

A solution (ca. 100 cm^3) of phosphate buffer in water/ethanol (50/50, v/v) (0.1 M, pH = 7.5) containing 5,10,15,20-tetrakis(2,3-dihydroxyphenyl)porphyrins (0.25 mmol) **1a–c** and **8** (1 mmol), was electrolyzed at 0.3 V versus 3 M Ag/AgCl in an undivided cell. The electrolysis was terminated when the current decreased by more than 95% of the initiated current. The process was interrupted during the electrolysis and the graphite anode was washed in acetone in order to reactivate it. At the end of the electrolysis, once the completion of the reaction was indicated by TLC, a few drops of phosphoric acid were added to the solution and the cell was placed in a refrigerator overnight. The precipitated solid was separated by filtration, washed with water and purified by recrystallization in dichloromethane/ethanol. After purification, the products **7a–c** were characterized by UV–vis, IR, ^{1}H NMR, ^{13}C NMR, mass spectroscopy and elemental analysis.

2.3. Characteristic of *7a*

Yield 66%, $IR_{(KBr)}$: 3375, 3304, 2958, 2586, 1603, 1511, 1462, 1402, 1282, 1267, 1217, 1141, 1082, 1029, 930, 760. UV–vis (DMF): λ_{max}/nm (log ε): 415(5.6), 509(4.6), 584(4.1), 641(3.9). ^{1}H NMR (300 MHz, DMSO-d_6, 25 °C): δ, ppm −2.84 (s, 2H, porphyrin N–H), 3.81 (s, 4H, N–H), 6.38(d, 4H, Ar–H), 6.98 (d, 4H, Ar–H), 7.21 (dd, 4H, Ar–H), 7.30 (dd, 4H, Ar–H), 7.69 (s, 4H, porphyrin Ar–H), 8.75(s, 8H, pyrrole-H), 9.51(s, 8H, OH). ^{13}C NMR(75 MHz, DMSO-d_6, 25 °C): δ, ppm 180.4, 149.0, 148.2, 147.1, 142.1, 133.5, 128.7, 128.1, 125.2, 122.5, 116.0, 112.7, 112.1, 103.2, 98.3. Elemental analysis Calc. for $C_{68}H_{42}N_8O_{12}$: C, 70.22; H, 3.64; N, 9.63; Found C, 70.19; H, 3.69; N, 9.68%. MALDI-TOF calcd m/z = 1162.29 $[M]^+$, found 1162.25.

2.4. Characteristic of *7b*

Yield 60%, $IR_{(KBr)}$: 3410, 3302, 2924, 2852, 1654, 1590, 1493, 1464, 1422, 1393, 1269, 1200, 1169, 838, 756, 695, 581, 540, and 461. UV–vis (DMF): λ_{max}/nm (log ε): 414(5.5), 512(4.5), 544(4.11), 587(4.0), 642(3.70).^{1}H NMR (300 MHz, DMSO-d_6, 25 °C): 3.81 (s, 4H, N-H), 6.35(d, 4H, Ar–H), 6.83 (d, 4H, Ar–H), 7.38 (dd, 4H, Ar–H), 7.48(dd, 4H, Ar–H), 7.71 (s, 4H, porphyrin Ar–H), 8.74(s, 8H, pyrrole-H), 9.55(s, 8H, OH). ^{13}C NMR(75 MHz, DMSO-d_6, 25 °C): δ, ppm 180.6, 149.3, 148.6, 147.8, 142.3, 134.1, 129.2, 128.4, 125.7, 123.1, 116.3, 113.2, 112.4, 103.8, 98.8. Elemental analysis Calc. for $C_{68}H_{40}N_8O_{12}Zn$: C, 66.59; H, 3.29; N, 9.14%; Found C, 66.55; H, 3.32; N, 9.17%. MALDI-TOF calcd m/z = 1224.21 $[M]^+$, found 1224.15.

2.5. Characteristic of *7c*

Yield 57%, $IR_{(KBr)}$: 3410, 3304, 2922, 1652, 1600, 1497, 1466, 1424, 1271, 1201, 1170, 1112, 840, 757, 697, 582, 541, and 462. UV–vis (DMF): λ_{max}/nm (log ε): 425(5.4), 473(5.1). Paramagnetic ^{1}H NMR (300 MHz, DMSO-d_6) δ, ppm −34.8 (β-pyrolic-H), 3.82 (N-H), 6.15–7.7(aromatic-H), 9.4(phenolic OH), elemental analysis Calc. for $C_{70}H_{43}MnN_8O_{14}$: C, 65.94; H, 3.40; N, 8.79; % Found C, 65.98; H, 3.42; N, 8.75%. MALDI-TOF calcd m/z = 1215.21 [M-acetate]$^+$, found 1215.20.

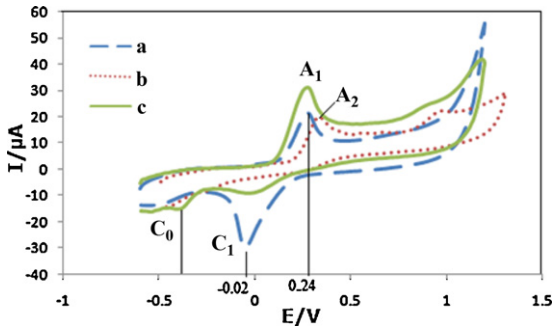

Fig. 1. Cyclic voltammograms of: (a) 0.25 mmol dm^{-3} of **1c**, (b) 1.0 mmol dm^{-3} of compound **8** and (c) mixture of 1.0 mmol dm^{-3} **8** and 0.25 mmol dm^{-3} of **1c** at a glassy carbon electrode (1.8 mm diameter) versus Ag/AgCl/3 M KCl as reference electrode, in 0.1 M phosphate buffer in water/ethanol (50/50, v/v) (pH = 7.5) solution. Scan rate = 100 mV s^{-1}, t = ambient.

3. Result and discussion

3.1. Electrochemical study of *1a–c* in the presence of *8*

The cyclic voltammogram of a 0.25 mM **1c** in water/ethanol (50/50) solution containing 0.1 M phosphate buffer (pH = 7.5), at a bare glassy carbon electrode, showed an oxidation peak at 0.23 V versus 3 M Ag/AgCl electrode. As can be seen in Fig. 1, curve a, a cathodic peak C_1 appeared in the reverse scan at −0.02 V vs. 3 M Ag/AgCl, illustrating the partial reversibility of the eight electron transfer process (four independent E mechanisms) that could be assigned to the **1c** and **2c** redox complex.

A peak current ratio ($I_p^{C_1}/I_p^{A_1}$) of more than unity (about 1.2) could be considered as a criterion for the stability of *o*-benzoquinone derivatives of **1c** produced at the surface of the electrode under the mentioned experimental conditions and partial adsorption of **2c** and/or **4c** at the surface of electrode. It is noteworthy that hydroxylation, ethoxylation [29,30], dimerization and polymerization [31,32] reactions are too slow to be observed on the time scale of cyclic voltammetry.

The electrooxidation of **1c** in the presence of **8** as a nucleophile was studied in some detail. Fig. 1, curve c shows the first cyclic voltammogram obtained for a 0.25 mM solution of **1c** in the presence of 1 mM of **8**. The voltammogram exhibits two cathodic peaks C_1 and C_0 (−0.35 V versus 3 M Ag/AgCl). In the second cycle (Fig. 2, curve b) a new anodic peak (A_0) appears with an E_p value of −0.32 V versus 3 M Ag/AgCl. This new peak is related to the oxidation of intermediate **4c** via four nearly reversible two electron processes (four independent E mechanisms). The decrease of peak C_1 in the cyclic voltammograms of **1c** in the presence of **8** clearly indicated that the electrochemical oxidation of **1c** was followed by chemical reactions with **8**. In addition the increase of peak A_1 in this voltammogram is due to the overlap of the quasireversible oxidation peak (A_2) of **8** with porphyrin **1c** oxidation peak. Fig. 1, curve b shows the cyclic voltammogram of **8** for comparison.

It seems that in each electrochemical step of this study, the second, third and fourth two-electron oxidations shift to lower potentials (second, third and fourth electron transfers are assisted by the previous steps). Hence the oxidation and reduction waves now involving four merged waves; appear like a single two-electron wave with respect to shape even although the height corresponds to 8-electron process for each electrochemical step [33,34].

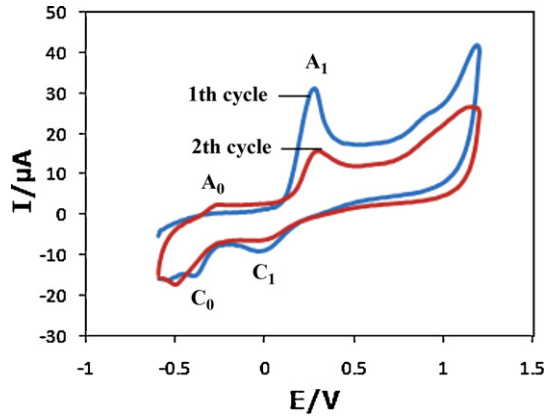

Fig. 2. Multi-cyclic voltammograms of 0.25 mmol dm^{-3} **1c** in the presence of 1.0 mmol dm^{-3} **8**, at glassy carbon electrode (1.8 mm diameter) versus Ag/AgCl/3 M KCl as reference electrode, in 0.1 M phosphate buffer in water/ethanol (50/50, v/v) (pH = 7.5) solution. Scan rate = 100 mV s^{-1}, *t* = ambient.

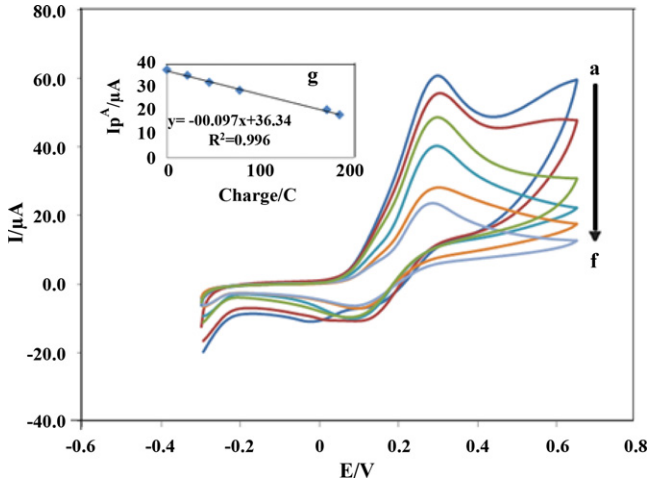

Fig. 4. Cyclic voltammograms of 0.25 mmol dm^{-3} **1c** in the presence of 1 mmol dm^{-3} **8** in 0.1 mol dm^{-3} phosphate buffer (pH = 7.5) in water/ethanol (50/50, v/v) solution at a glassy carbon electrode, during controlled potential coulometry at 0.3 V versus Ag/AgCl/3 M KCl. After consumption of: (a) 0, (b) 22, (c) 45 (d) 78 (e) 171 (f) 185 C. Inset: variation of peak current ($I_p^{A_1}$) vs. charge consumed. Scan rate = 100 mV s^{-1}, *t* = ambient.

The effect of the potential scan rate on the shape of cyclic voltammograms of **1c** in the presence of **8** was also studied. It can be seen that, proportional to the augmentation of the potential scan rate, the height of peak C_1 increases (Fig. 3, curves: a–f). A similar situation is observed when the **8** to **1c** concentration ratio is decreased. A plot of the peak current ratio ($I_p^{C_1}/I_p^{A_1}$) versus the scan rate for a mixture of **1c** and **8** confirms the reactivity of *o*-benzoquinone derivatives of **1c**, (**2c**) with **8**, appearing as an increase in the peak current ratio ($I_p^{C_1}/I_p^{A_1}$) at higher scan rates (Fig. 3, curve g). Furthermore, under these conditions, the current function for A_1 peak, ($I_p^{A_1}/v^{1/2}$) changes only slightly when increasing the scan rate (Fig. 3, curve h). Controlled potential coulometry was performed in a water/ethanol (50/50) phosphate buffer solution (*c* = 0.1 M, pH = 7.5), containing 0.1 mmol of **1c** and 0.4 mmol of 8 at 0.15 V versus 3 M Ag/AgCl. The monitoring of the electrolysis progress was done using cyclic voltammetry, it could be clearly observed that with the progress of the coulometry, anodic (A_1) and cathodic (C_1) peaks disappeared when the charge consumption became about 16 electrons per each molecule of **1c** (Fig. 4). Similar results were observed for the oxidation of **1a** and **1b** in the presence of **8**. Diagnostic criteria of cyclic voltammetry, the consumption of 16 electrons per molecules of **1a–c** and the spectroscopic data of the isolated product, indicated that the reaction mechanism of electrooxidation of **1a–c** in the presence of **8** is four independent ECEC mechanisms (electrochemical/chemical/electrochemical/chemical reactions) as illustrated in Scheme 1 [33].

On the basis of these observations one can suppose that **2a–c** is formed from **1a–c** by four *E* pathways, and then four Michael-additions of nucleophile **8** at C-5 of o-benzoquinone occur [15,35,36]. The formed o-diphenols in **4a–c** are oxidized such as **1a–c** in four *E* reactions to the o-benzoquinone **5a–c** and four intramolecular Michael-additions on this intermediate produces benzoquinones in **2a–c** (Scheme 1) seems to occur much faster than other side reactions leading presumably to the intermediates **4a–c**. The oxidation of the compounds **4a–c** at the A_0 peak potential followed by four intramolecular Michael additions [35–39] and parallel two proton shifts and aromatization at each phenyl ring (Scheme 1) lead to **7a–c** as the final products. The Michael acceptors **2a–c** are first attacked selectively by the –NH_2 group of **8** which has more nucleophilicity (not by oxygen) on the C-5 positions of the phenyl ring that have less hindrance, then by –OH of 8 on the C-6 positions [12,13,17]. The successful synthesis of the target materials **7a–c** was established via UV–vis, IR, ^{1}H NMR, ^{13}C NMR and MALDI-mass spectroscopic methods.

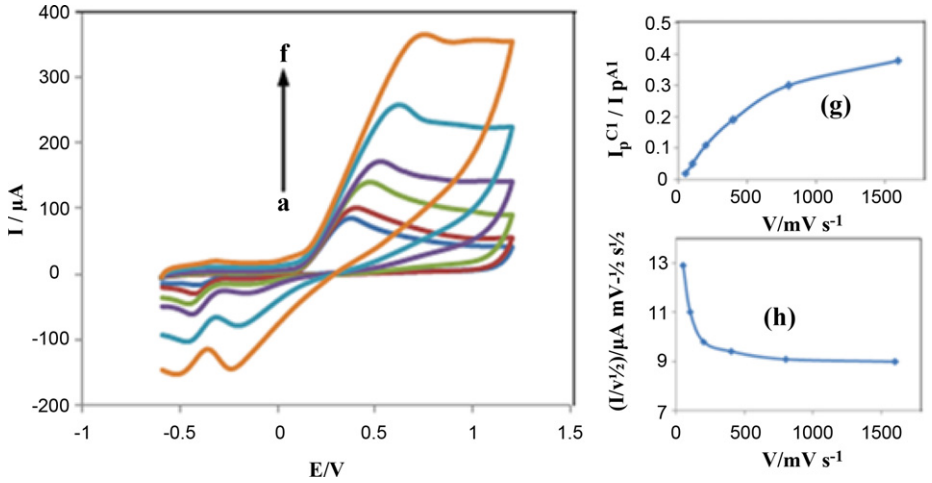

Fig. 3. Typical voltammograms of 0.25 mmol dm^{-3} **1c** in the presence of 1.0 mmol dm^{-3} **8** in 0.1 mol dm^{-3} phosphate buffer (pH = 7.5) in water/ethanol (50/50, v/v) solution at a glassy carbon electrode versus Ag/AgCl/3 M KCl as reference electrode and various scan rates. Scan rates from (a) to (f) are: 50, 100, 200, 400, 800, 1600 mV s^{-1}, respectively. Curve (g): variation of peak current ratio $I_p^{C_1}/I_p^{A_1}$ vs scan rate. Curve (h): variation of peak current function ($I_p^{A_1}/v^{1/2}$) vs scan rate, *t* = ambient.

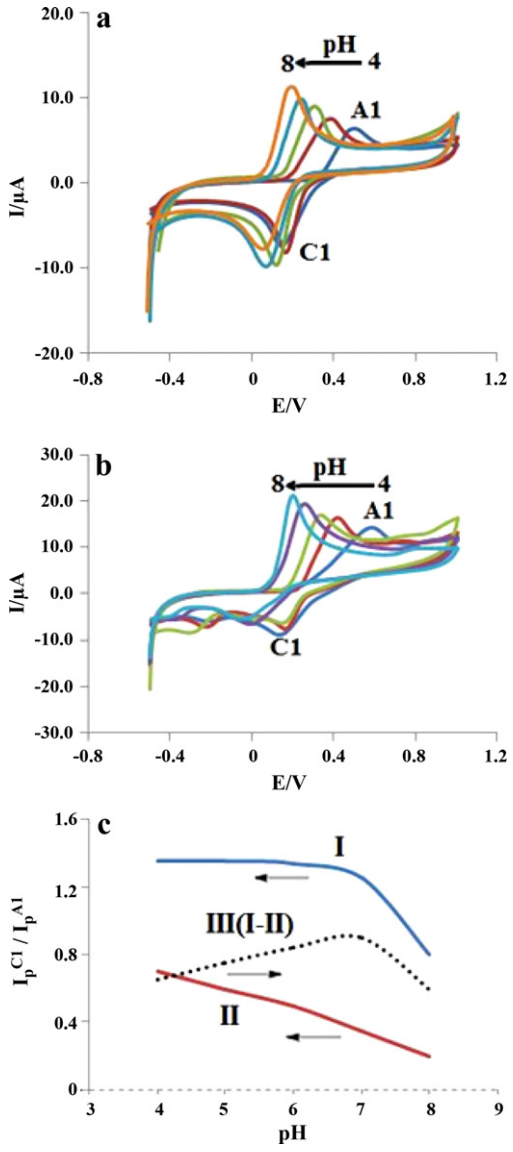

Fig. 5. (a) Cyclic voltammograms of 0.25 mmol dm^{-3} **1c** at different pHs versus Ag/AgCl/3 M KCl. (b) Cyclic voltammograms of 0.25 mmol dm^{-3} **1c** in the presence of 1 mmol dm^{-3} **8** at different pHs. (c) Curve (I), variation of peak–current ratio ($I_p^{C_1}/I_p^{A_1}$) of **1c** in the absence of **8**, curve (II), variation of peak current ratio ($I_p^{C_1}/I_p^{A_1}$) of **1c** in the presence of **8** and curve (III), difference between peak–current ratio ($I_p^{C_1}/I_p^{A_1}$) in the presence and absence of **8**.

3.2. The effect of pH

The voltammetric behavior of catecholes at various pHs are well known and were studied in various papers [40,41]. In this work the electrochemical oxidation of **1c** alone and in the presence of **8** were studied in different pHs. As Fig. 5a shows, the peak potential for peak A_1 shifted to the negative potentials by increasing the pH. This is expected because of the participation of protons in the oxidation of **1c** to **2c** and **4c** to **5c**.

$$R - 8e^- - mH^+ \leftrightarrow O$$

where R stands for **1c** and **4c**, O stand for **2c** and *m* is the number of protons involved in the reactions. The oxidation peak potential (for the A_1 peak) E_{ox} is given by:

$$E_{OX} = E^0_{OX} - \left(\frac{2.303mRT}{8F}\right) pH$$

where E^0_{OX} is the oxidation peak potential at pH = 0.0 and R, T and F have their usual meanings [42]. This figure and Fig. 5c, curve I also shows the ($I_p^{C_1}/I_p^{A_1}$) decrease when the pH increases. This is due to the coupling of monoanionic or dianionic forms of **1c** with their oxidized form **2c** in a dimerization or polymerization reaction [31,32]. The rate of the coupling reaction was pH dependent and enhanced by the increasing of pH. The cyclic voltammograms of **1c** in the presence of **8** showed that the peak–current ratio ($I_p^{C_1}/I_p^{A_1}$) increased with the decreasing of pH (Fig. 5b and c, curve (II)).

This can be related to the protonation of the enolate form of **8** and its subsequent inactivation towards Michael addition reaction. At pH = 7.5 the rate of dimerization and polymerization reaction is decreased (peak current ratio $I_p^{C_1}/I_p^{A_1}$ in the absence of **8** ~1.25) and the rate of the reaction between **8** and **2c** and **4c** is increased (peak current ratio $I_p^{C_1}/I_p^{A_1}$ in the presence of **8** ~0.35), see Fig. 4, curves I and II, respectively. Thus a solution of water/ethanol containing 0.1 M phosphate buffer (pH = 7.5) was the most suitable solvent system for electrochemical study and synthesis in this work.

3.3. Spectroscopic characterization of *7a–c*

The ^{1}H NMR spectra of the products confirm their formation. Assignments are made on the basis of previous assignments for 5,10,15,20-tetrakis (2,3-dihydroxyphenyl) porphyrin [34,43] and Mn (III) tetraaryl porphyrin [44] complexes, relative intensity and comparison with the pattern of signals in the starting materials. Phenyl protons of **7a–b** and **8** were split and were seen at 6.3–7.6. Intensities of the phenyl signals relative to the pyrrole signals were exactly 8–20 according to the related products. The disappearance of the OH proton of **8** at 9.01 is another distinct reason for the occurrence of the cyclization reaction. Mn (III) porphyrins with unfilled d shell of Mn (III) are paramagnetic. The observed chemical shifts of protons in paramagnetic molecules are due to a combination of diamagnetic and paramagnetic contributions. The paramagnetic shifts are caused by spin delocalization from the unpaired electron to the protons at the periphery of the molecule [45]. Paramagnetic ^{1}H NMR of **7c** shows β-pyrolic-Hs that appear at −34.8 ppm and protons of the phenyls periphery appear as multiplet between 6.15 and 7.7 ppm [45].

The attachment of four units of **8** to porphyrin **7a** and **7b** produced 15 signals in the ^{13}C NMR spectrum, while less symmetric porphyrins with one, two or three units of **8** were expected to have more signals. The signals related to C–OH carbons of **7a–b** were seen at 149.3 and 148.6 ppm, respectively. The FT-IR spectra of products exhibit characteristic peaks of **1a–c** and **8** according to literature [34].

3.3.1. UV–vis and fluorescence

The absorption spectra of compounds **7a–c** along with **1a–c** in methanol are shown in Fig. 6. Compound **8** does not have any absorption in this region. The band at about 415 nm is the soret band of the porphyrin moiety, which is an $a_{1u}(\pi) \rightarrow e_g(\pi^*)$ electron transition, assigned to the second excited state S_2 generated by the $\pi \rightarrow \pi^*$ transition. The weak absorption bands between 500 nm and 660 nm are the Q bands of the porphyrin moiety and correspond to an $a_{2u}(\pi) \rightarrow e_g(\pi^*)$ electron transition, belonging to the first excited state S_1 generated by $\pi \rightarrow \pi^*$ transition [46,47]. The soret absorption wavelength of **7a** is almost identical with porphyrin **1a** but the intensity of the **7a** soret band is stronger as a result of π electron density extension of the HOMO π system by the aminophenol ring. Absorption spectrum of **1b** has some differences relative to **7b**. On the other hand, the soret band of **7b** is stronger and blue-shifted by 11 nm and its Q bands intensified compared to those of the parent porphyrin. UV–vis spectrum of **7c** is blue shifted about 50 nm and intensified compared to **1c**. These blue shifts are more

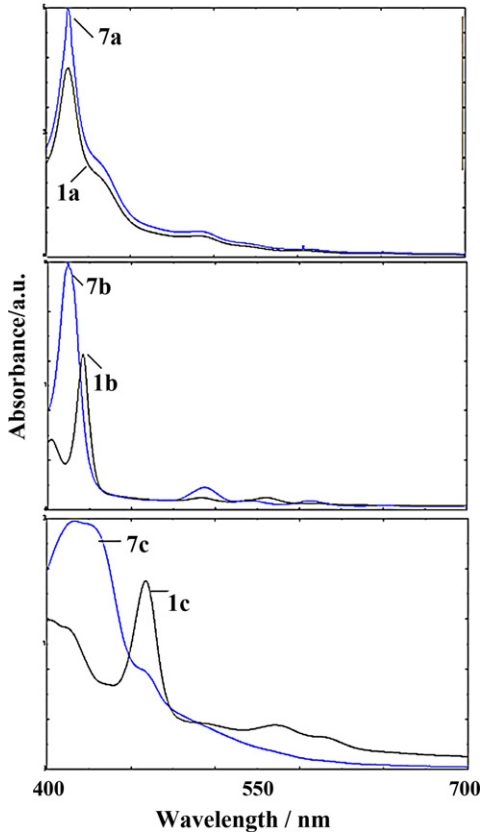

Fig. 6. UV–vis spectra of **1a–c** and **7a–c** in methanol at concentration of 10^{-5} mol dm^{-3}.

pronounced in **7c** compared to **7b**. The metallation of the free base porphyrin by manganese results in considerable red shift due to the effective π interaction between metal d orbital's and porphyrin π system [48]. Blue shifts in **7b** and **7c** show that the effective interaction between metals and the porphyrin ligand is considerably decreased due to the strong deformation of the porphyrins caused by steric hindrance of the phenoxazine substitutions. Another feature of the UV–visible spectrum of **7c** is its broadness that indicates atropoisomerism resulting from bulky substitution on the phenyls [49]. This indicates the substituent's significantly affecting the photophysical nature of the metalloporphyrin core. The results of these study show that electrosynthesized materials **7a–c** could be better candidate for designing light harvesting materials that operate over a greater range of the solar spectrum compared to simple, well-studied less functionalized porphyrin chromophores alone.

The fluorescence spectra of the **1a**, **8** and **7a** are shown in Fig. 7. These compounds were excited at 400 nm, where the porphyrin subunit absorbs strongly. The emission spectrum of **7a** shows characteristic luminescence of the metal-free porphyrin cores at 635 nm and 690 nm that was quenched by 50% in comparison with **1a** at equal concentration. Compounds **8** and **1a** show a very weak emission at about 460 nm that appears in the emission spectra of **7a** without any shift but notably decreases in intensity. This decrease supports the energy transfer from the porphyrin core excited state to the four **8** groups as the electron acceptor subunits in **7a** [50].

Of the metalloporphyrins, the zinc porphyrin **1b** emitted fluorescence; the emission peaks were situated at 580 and 635 nm which was some 55 nm blue shifted compared to the metal-free porphyrins. The fluorescence intensity of **1c** is 15 times less than its metal-free counterpart's because Mn^{III} is a paramagnetic ion with an unfilled d shell and could strongly quench the fluorescence of

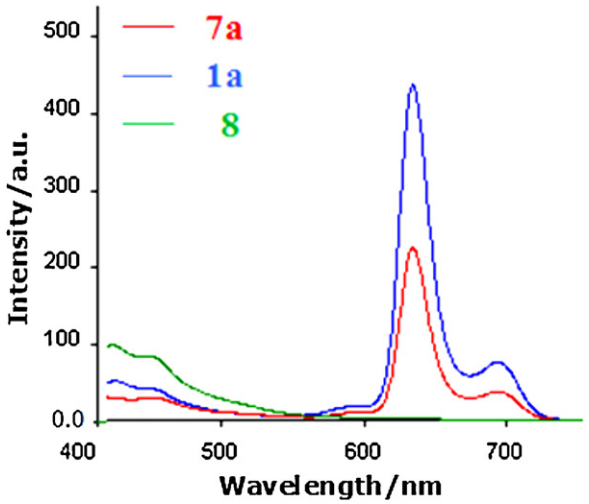

Fig. 7. Fluorescence spectra of compounds **1a**, **8** and **7a** in methanol at concentration of 10^{-5} mol dm^{-3}, λ_{exc} = 400 nm.

the fluorophore near it via electron or energy transfer [51]. Thus the order of fluorescence intensity of the porphyrins was **1a** > **1b** ≫ **1c**.

When **7b** and **7c** were excited at 400 nm the emission of the porphyrins were quenched and had not been detected under the particular experimental conditions used.

3.4. SEM

The synthetic versatility of porphyrins allows the preparation of molecular units capable of assembling in ordered supramolecular structures, characterized by different geometrical motifs [52–54]. The morphology and size of the samples were further investigated using scanning electron microscopy (SEM). SEM images indicate that this method produces regular shapes of manganese porphyrin nano-particles and most of the crystals of **7c** posses a cubic nano structure with a dimension of about 100 nm (Fig. 8). Synthesis of nanosized materials usually needs further treatment such as hydrothermal and sonification [55–57] but in our work nano-particles were deposited directly on the electrode during electrosynthesis without using other techniques.

To the best of our knowledge, this is a novel method for the synthesis of nano-sized structures of functionalized manganese porphyrins during electrosynthesis.

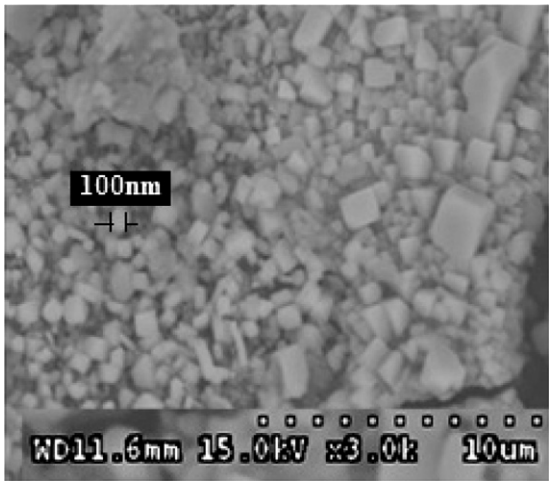

Fig. 8. SEM image of **7c** shows that most of crystals have cubic nano structures.

4. Conclusion

In conclusion, the phenoxazine-porphyrin catechol compounds were successfully synthesized and characterized. At first porphyrin-catecholes **1a–c** are oxidized to their respective *o*-benzoquinones **2a–c**. The formed *o*-benzoquinones are attacked by four equivalent **8**, via four independent *ECEC* mechanisms, including two Michael addition reactions and two parallel or sequential eliminations of hydrogen followed by intramolecular cyclization, converted to **7a–c** as the final products. The combination of the novel properties of porphyrins, catecholes and phenoxazine and the formation of π-extended heterocyclic fused porphyrins is the major advantage of this research that can possibly create useful properties. This strategy can be used for the synthesis of additional new functionalized porphyrins.

Acknowledgements

This work was supported by the Iranian National Science Foundation (INSF) and Shahid Beheshti University Research Affaires.

References

[1] K.M. Kadish, K.M. Smith, R. Guilard, The Porphyrin Handbook, vol. 3, Academic Press, 2000 (Ch. 21).
[2] D. Gust, T.A. Moore, A. Moore, Acc. Chem. Res. 42 (2009) 1890.
[3] N. Aratani, D. Kim, A. Osuka, Acc. Chem. Res. 42 (2009) 1922.
[4] C.L. Peng, P.S. Lai, C.C. Chang, P.J. Lou, M.J. Shieh, Dyes Pigments 84 (2010) 140.
[5] J.K. Park, J. Chen, H.R. Lee, S.W. Park, H. Hinokubo, T. Osuka, D. Kim, J. Phys. Chem. 113 (2009) 21956.
[6] S. Zhao, M.G.P.M.S. Neves, A.C. Tome, A.M.S. Silva, J.A.S. Cavaleiro, M.R.M. Domingues, A.J.F. Correia, Tetrahedron Lett. 46 (2005) 2189.
[7] N.M. Boyle, J. Rochford, M.T. Pryce, Coord. Chem. Rev. 254 (2010) 77.
[8] H. Boedigheimer, G.M. Ferrence, T.D. Lash, J. Org. Chem. 75 (2010) 2518.
[9] M. Zhu, M. Han, Y. Du, P. Yang, X. Wang, Dyes Pigments 86 (2010) 81.
[10] S. Osati, N. Safari, P.R. Jamaat, Inorg. Chim. Acta 363 (2010) 2180.
[11] N.K.S. Davis, A.L. Thompson, H.L. Anderson, J. Am. Chem. Soc. 133 (2011) 30.
[12] S.S. Hosseiny Davarani, A.R. Fakhari, N. Sheijooni Fumani, M. Kalate-bojdi, Electrochem. Commun. 10 (2008) 1765.
[13] M. Shamsipur, S.S. Hosseiny Davarani, M. Nasiri-Aghdam, D. Nematollahi, Electrochim. Acta 51 (2006) 3327.
[14] A. Bayandori Moghaddam, F. Kobarfard, A.R. Fakhari, D. Nematollahi, S.S. Hosseiny Davarani, Electrochim. Acta 51 (2005) 739.
[15] S.S. Hosseiny Davarani, D. Nematollahi, M. Shamsipur, N. Mashkouri Najafi, L. Masoumi, S. Ramyar, J. Org. Chem. 71 (2006) 2139.
[16] D. Nematollahi, A. Amani, E. Tammari, J. Org. Chem. 72 (2007) 3646.
[17] D. Nematollahi, D. Habibi, M. Rahmati, M. Rafiee, J. Org. Chem. 69 (2004) 2637.
[18] S.S. Hosseiny Davarani, S. Ramyar, L. Masumi, N. Sheijooni Fumani, A. Bayandori Moghadam, J. Electrochem. Soc. 155 (2008) 120.
[19] A. Bolognese, G. Correale, M. Manfra, A. Lavecchia, O. Mazzoni, E. Novellino, V. Barone, P. Colla, R. Loddo, J. Med. Chem. 45 (2002) 5217.
[20] W. Muller, D.M. Crothers, Eur. J. Biochem. 54 (1975) 267.
[21] B.C. Channu, H.N. Kalpana, G.B. Eregowda, C. Dass, P.J. Houghton, K.N. Thimmaiah, J. Pharm. Biomed. Anal. 21 (1999) 775.
[22] G.P. Moloney, Magn. Reson. Chem. 28 (1990) 824.
[23] F.P. Scheafer (Ed.), Dye Lasers, Springer-Verlag, Berlin, 1973.
[24] M. Pauchard, S. Huber, R. Meallet-Renault, H. Maas, R. Pansu, G. Calzaferri, Angew. Chem. Int. Ed. 40 (2001) 2839.
[25] G. Calzaferri, H. Maas, M. Pauchard, M. Pfenniger, S. SonsMegelski, A. Devaux, Advances in Photochemistry, vol. 27, John Wiley & Sons Inc., Hoboken, 2002, p. 1.
[26] A. Wiehe, E.J. Simonenko, M.O. Senge, B. Röder, J. Porphyrins Phthalocyanines 5 (2001) 758.
[27] S.A. Syrbu, A.S. Semeikin, Russ. J. Org. Chem. 35 (1999) 1236.
[28] D.A. James, D.P. Arnold, P.G. Parsons, Photochem. Photobiol. 59 (1994) 441.
[29] L. Papouchado, G. Petrie, J.H. Sharp, R.N. Adams, J. Am. Chem. Soc. 90 (1968) 5620.
[30] L. Papouchado, G. Petrie, R.N. Adams, J. Electroanal. Chem. 38 (1972) 389.
[31] R.E. Sioda, B. Frankowska, J. Electroanal. Chem. 568 (2008) 356.
[32] S.S. Hosseiny Davarani, N. Sheijooni Fumani, H. Arvin-Nezhad, F. Moradi, Tetrahedron Lett. 49 (2008) 710.
[33] A.J. Bard, L.R. Faulkner, Electrochemical Methods, 2nd ed., Wiley, New York, 2001, p. 469, 246, 497.
[34] P.R. Jamaat, S.S. Hosseiny Davarani, N. Sheijooni Fumani, L. Masoumi, N. Safari, J. Porphyrins Phthalocyanines 12 (2008) 85.
[35] S.S. Hosseiny Davarani, N. Mashkouri Najafi, S. Ramyar, L. Masoumi, M. Shamsipur, Chem. Pharm. Bull. 54 (7) (2006) 959.
[36] D. Nematollahi, M. Hesari, J. Electroanal. Chem. 557 (2005) 197.
[37] M.R. Islami, Z. Hassani, H. Sheibani, B. Abdolahzadeh, N. Etminan, Tetrahedron 59 (2003) 4993.
[38] D. Nematollahi, M. Rafiee, H.R. Khavasi, Bull. Chem. Soc. Jpn. 81 (11) (2008) 1505.
[39] I. Yavari, M. Adib, L. Hojabri, Tetrahedron 58 (2002) 6895.
[40] D. Nematollahi, M. Rafiee, J. Electroanal. Chem. 566 (2006) 31.
[41] M. Rafiee, D. Nematollahi, J. Electroanal. Chem. 626 (2009) 36.
[42] H. Salehzadeh, D. Nematollahi, M. Rafiee, J. Electroanal. Chem. 650 (2011) 226.
[43] S. Osati, N. Safari, M. Kalate Bojdi, S.S. Hosseiny Davarani, J. Electroanal. Chem. 655 (2011) 120.
[44] N. Safari, B. Notash, J. Mohammad Nezhad, H. Chiniforoshan, H. Hadadzadeh, A.R. Rezvani, Inorg. Chim. Acta 358 (2005) 2967.
[45] E. Ben-Hur, W.S. Chan, K.M. Kadish, K.M. Smith, R. Guilard (Eds.), The Porphyrin Handbook, vol. 5, 2003, p. 88, 157.
[46] J. Rodriguez, C. Kirmaier, D. Holten, J. Am. Chem. Soc. 111 (1989) 6500.
[47] S. Fukuzumi, Y. Endo, Y. Kashiwagi, Y. Araki, O. Ito, H. Imahori, J. Phys. Chem. B 107 (2003) 1979.
[48] K.M. Kadish, K.M. Smith, R. Guilard, The Porphyrin Handbook, vol. 3, Academic Press, 2000, p. 59.
[49] R.F. Beeston, S.E. Stitzel, M.A. Rhea, J. Chem. Educ. 74 (1997) 1468.
[50] X. Qiu, R. Lu, H. Zhou, X. Zhang, T. Xu, X. Liu, Y. Zhao, Tetrahedron Lett. 49 (2008) 7446.
[51] G. Szintay, A. Horvath, Inorg. Chim. Acta 324 (2001) 278.
[52] C.M. Drain, G. Smeureanu, S. Patel, X. Gong, J. Garno, J. Arijeloye, New J. Chem. 30 (2006) 1834.
[53] X. Gong, T. Milic, C. Xu, J.D. Batteas, C.M. Drain, J. Am. Chem. Soc. 124 (2002) 14290.
[54] Z. Ou, H. Yao, K. Kimura, Photochem. Photobiol. A 189 (2007) 7.
[55] A. Gedanken, Ultrason. Sonochem. 11 (2004) 47.
[56] E. Lester, P. Blood, J. Denyer, D. Giddings, B. Azzopardi, M. Poliakoff, J. Supercrit. Fluids 37 (2006) 209.
[57] H. Sadeghzadeh, A. Morsali, Ultrason. Sonochem. 18 (2011) 80.